Screening Platform for Cell Contact Guidance Based on Inorganic Biomaterial Micro/nanotopographical Gradients

Zhou, Qihui; Castañeda Ocampo, Olga; Guimarães, Carlos; Kuhn, Philipp; van Kooten, Theo; van Rijn, Patrick

Published in:
ACS Applied Materials & Interfaces

DOI:
10.1021/acsami.7b08237

Publication date:
2017

ACS APPLIED MATERIALS & INTERFACES

Research Article

www.acsami.org

Screening Platform for Cell Contact Guidance Based on Inorganic Biomaterial Micro/nanotopographical Gradients

Qihui Zhou,[†,‡] Olga Castañeda Ocampo,[§,∥] Carlos F. Guimarães,[†] Philipp T. Kühn,[†,‡] Theo G. van Kooten,[†,‡] and Patrick van Rijn*[,†,‡,§]

[†]Department of Biomedical Engineering—FB40, University of Groningen, University Medical Center Groningen, Groningen, A. Deusinglaan 1, 9713 AV Groningen, The Netherlands

[‡]W.J. Kolff Institute for Biomedical Engineering and Materials Science—FB41, University of Groningen, University Medical Center Groningen, Groningen, A. Deusinglaan 1, 9713 AV Groningen, The Netherlands

[§]Zernike Institute for Advanced Materials, University of Groningen, Nijenborgh 4, 9747 AG Groningen, The Netherlands

[∥]Stratingh Institute for Chemistry, University of Groningen, Nijenborgh 4, 9747 AG Groningen, The Netherlands

Supporting Information

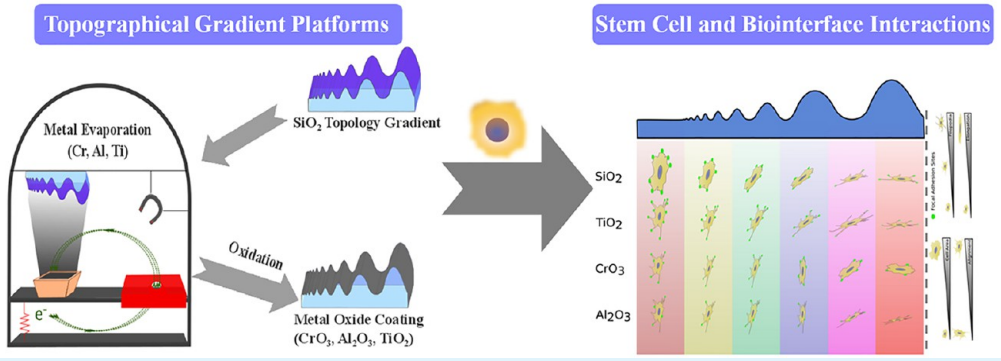

ABSTRACT: High-throughput screening (HTS) methods based on topography gradients or arrays have been extensively used to investigate cell−material interactions. However, it is a huge technological challenge to cost efficiently prepare topographical gradients of inorganic biomaterials due to their inherent material properties. Here, we developed a novel strategy translating PDMS-based wrinkled topography gradients with amplitudes from 49 to 2561 nm and wavelengths between 464 and 7121 nm to inorganic biomaterials (SiO_2, Ti/TiO_2, Cr/CrO_3, and Al_2O_3) which are frequently used clinical materials. Optimal substratum conditions promoted human bone-marrow derived mesenchymal stem cell alignment, elongation, cytoskeleton arrangement, filopodia development as well as cell adhesion in vitro, which depended both on topography and interface material. This study displays a positive correlation between cell alignment and the orientation of cytoskeleton, filopodia, and focal adhesions. This platform vastly minimizes the experimental efforts both for inorganic material interface engineering and cell biological assessments in a facile and effective approach. The practical application of the HTS technology is expected to aid in the acceleration of developments of inorganic clinical biomaterials.

KEYWORDS: *high-throughput screening, topographical gradient, inorganic biomaterials, biomimetic surface, stem cell behavior*

1. INTRODUCTION

Over the past decades, it has been demonstrated that cells can sense and respond to their microenvironment, especially physical stimuli (e.g., shear stress,[1] stiffness,[2] and topography[3])) and insoluble/soluble chemical signals (e.g., material component,[4] extracellular matrix (ECM) proteins,[5] and growth factors[6]) as well as adjacent cells.[7] Among physical cues, surface micro/nanotopography serves as an important indirect signal that strongly influences cell behavior and function through a process known as mechanotransduction.[8,9] For instance, microtopographies such as micrograting guide the shape and motility of the cell body by physical confinement or alignment and typically result in whole-cell contact guidance.[10−12] In contrast, nanotopographies are several orders of magnitude smaller than the cell body but have a size similar to that of subcellular structures (e.g., F-actin, filopodia, and integrin receptors). It may therefore be possible to target transmembrane receptor proteins involved in intracellular signal transduction and thus manage the response of the anchorage-dependent cells.[13−15] To date, cells can "feel" and interact with the smallest feature size of a substrate at approximately 5 nm.[14] It is important to address both nano- and microtopographies as

Received: June 8, 2017
Accepted: August 21, 2017
Published: August 21, 2017

DOI: 10.1021/acsami.7b08237
ACS Appl. Mater. Interfaces 2017, 9, 31433−31445

was shown by Bae et al., who did competition experiments using fibroblasts. They found that the morphologies and orientations of fibroblasts were clearly affected by the nanotopography rather than the microtopography.[16] In the field of biomaterials, biomimetic topographical patterns modulate cell behavior and promote tissue regeneration.[17] In particular, most tissue extracellular matrixes (e.g., bone, tendon, nerve, myocardium, etc.) have regular and anisotropic architectures consisting of well-aligned micro/nano-scaled fibrous structures.[18−21] Increasing evidence suggests that an aligned topographical structure is essential for cell alignment and tissue morphogenesis as well as remodeling to allow the effective and accurate expression of tissue functions.[22−24] Therefore, establishing precise topographical features is very critical for cell behavior, function, and protein expression. However, many of these studies focused on independent substrates with varying dimensions or structures including pillars, pores, or grooves, which provided interesting yet limited information.

Surface topographical gradients offer an ideal platform to address high-throughput screening (HTS) of cell behavior toward topography. This approach is time and cost efficient, elicits more accurately the optimum topographical conditions for promoting cellular processes, and minimizes systematic or methodological errors.[25−29] Faia-Torres et al. applied polycaprolactone roughness gradient as a platform to identify the impact of roughness on osteogenic fate of stem cells in vitro. An optimal substrate roughness range ($R_a \sim 2.1-3.1\ \mu m$) for promoting the osteogenic cell differentiation and an $R_a \sim 0.93\ \mu m$ for more effectively supporting the osteogenic expression in osteogenic induction medium was found.[26,30] Kim et al. developed many poly(urethane acrylate) gradient platforms of anisotropic or isotropic topographical patterns to investigate the organization, alignment, topotaxis, and phenotypic development of different cell types.[27,28,31,32] However, most of investigations mainly focused on soft or elastic polymers, which limits the use of these platforms as in many orthopedic, orthodontic, and dental applications, for which inorganic biomaterials (e.g., metals, metal oxides, bioceramics, and bioglass) are used. These inorganic biomaterials have good biocompatibility, excellent mechanical properties, and superior corrosion resistance but are limited due to their bioinert surface properties or lack of bioactive signals.[12,33] It has been reported that bioinert ceramics (e.g., Al_2O_3) are unable to promote bone formation and osseointegration, both of which are major challenges for bone implants.[12,34] Webster et al. showed that the proliferation, adhesion, and mineralization differentiation of osteoblasts increased on nanostructured (<100 nm) bioinert alumina ceramics compared with conventional ceramics (surface structures >100 nm).[33,35] The opposite behavior was found for fibroblasts, which is beneficial because fibroblasts contribute to fibrous encapsulation and callus formation, events that may lead to implant loosening.[36] Topographical preparation techniques for inorganic biomaterials include anodization,[37] acid etching,[38] erosion,[39] inkjet printing,[12] and photolithography,[40] which enables micro- and/or nanotopographical features (e.g., ripples, grooves, islands, or pillars). However, most of these techniques only result in random or uniform surface structures, preventing the determination of optimum surface features to direct cell responses. Therefore, translating the topographical gradient with biomimetic patterns and dimensions to inorganic biomaterials provides significant technological advances for biomaterial development. Here, we address the translation of aligned nano/microtopography gradients to alumina (Al_2O_3) as bioceramic, titanium dioxide (TiO_2), and chromium oxide (CrO_3) for metal oxides of which the surface of titanium and cobalt/chrome implants are composed of, respectively, and silica (SiO_2) as a bioglass representative.

We developed a multiscale topographical gradient approach with different inorganic biomaterials by combining polydimethylsiloxane (PDMS) wrinkle gradients (amplitudes = 49−2561 nm; wavelengths = 464−7121 nm) prepared by a masked plasma-oxidation procedure with subsequent overoxidation to obtain a SiO_2-like surface or metal evaporation, resulting in metal oxides (TiO_2, CrO_3, and Al_2O_3) upon exposure to air. The wrinkle dimension and surface chemistry were systematically examined by atomic force microscopy (AFM) and X-ray photoelectron spectroscopy (XPS), respectively. The topographical gradients of different inorganic biomaterials were seeded with human bone marrow derived mesenchymal stem cells (hBM-MSCs) to study the effects of wrinkle dimensions and biomaterial composition on cellular responses, including cell adhesion, spreading, morphology changes (e.g., elongation and orientation), cytoskeleton, filopodia as well as formation and orientation of focal adhesion contacts.

2. METHODS

2.1. PDMS Film Preparation. The PDMS slab was prepared by mixing the prepolymer and cross-linker (Sylgard 184, Dow Corning) in a ratio of 10:1 by weight according to the supplier's information. The 33 g mixture was vigorously stirred with a spatula. Once thoroughly mixed, the viscous mixture was degassed for 15 min under vacuum to remove the air bubbles completely and poured into a carefully cleaned, 12 × 12 cm squared polystyrene Petri dish to ensure equally thick samples. The Petri dish with liquid PDMS was cured in a vacuum oven at 70 °C overnight to cross-link into an elastomer. After curing, the elastomer slab was peeled away from the dish and cut into the desired size.

2.2. Preparation of Wrinkled Gradients with Silicone Oxide (SiO_2) and Metal Oxide Surfaces. For wrinkled gradient with SiO_2 surface, the PDMS sample was placed in a homemade stretching apparatus and stretched uniaxial to a strain of 30% of their original length. Stretched PDMS was partly covered with a mask (1.3 cm) and oxidized in air plasma under the stable pressure (Plasma Activate Flecto 10 USB, maximum intensity). After oxidation, the strain was released which induces wrinkled gradient formation with different wavelength and amplitude. The approach was based on our previous investigation.[25] All samples were post-treated with air plasma for 10 min to ensure that the surface is fully oxidized (maximum SiO_2 formation) and that surface chemistry as well as stiffness is equal for all samples.

The PDMS samples with wrinkled gradients and the controls were fastened on a metal stage and placed into a home-built thermal evaporator. A 5 nm layer of Cr was first evaporated in order to improve the adhesion of metals on oxidized PDMS. An initial rate of 0.3 Å/s was set until constant deposition was observed and then ramped to 0.2 and 0.4 Å/s. Subsequently, a 10 nm layer of metal (Ti or Al) was thermally evaporated. The rates of each metal are dependent on their melting temperatures. For aluminum, which has the lowest melting temperature in this particular process, only one rate of 0.2 Å/s was necessary. For Cr, a layer of 10 nm was directly formed. The process was performed under vacuum, and a temperature of 23−28 °C was maintained throughout. Voltage was applied and varied according to conditions. The thickness of the layer was measured during the process through the use of a quartz crystal inside the vacuum chamber. The thickness is read through the change in oscillation frequency of the crystal (it drops) as its mass is increased by the material being evaporated. An electronic instrument continuously

DOI: 10.1021/acsami.7b08237
ACS Appl. Mater. Interfaces 2017, 9, 31433−31445

reads the frequency and converts it to thickness, both instantaneous and cumulative.

2.3. Atomic Force Microscopy (AFM). AFM images were obtained using a commercial atomic force microscope (Nanoscope V Dimension 3100 microscope, Veeco, United States) operating with the tapping mode in air. The wavelength and amplitude of wrinkles in these images were analyzed by NanoScope Analysis software. The Young's modulus was measured by BioScope Catalyst AFM instrument (Bruker, Billerica, MA, United States) with NanoScope Analysis software. All measurements were performed in the quantum-mechanical nanomapping mode with a large amplitude using Bruker SCANASYST-AIR cantilevers made from silicon nitride with silicon made tips.

2.4. X-ray Photoelectron Spectroscopy (XPS). The coated metals above were determined using XPS (S-Probe, Surface Science Instruments, Mountain View, CA, United States) equipped with an aluminum anode (10 kV, 22 mA). Samples were placed in the prevacuum chamber of the XPS and then subjected to a vacuum of 10^{-9} Pa. X-rays (10 kV, 22 mA) at a spot size of 250 × 1000 μm were produced using an aluminum anode. Scans of the overall spectrum in the binding energy range of 1−1100 eV were made at low resolution (pass energy 150 eV).

2.5. Water Contact Angle (WCA) Measurement. To evaluate the wettability of flat surfaces with SiO_2, TiO_2, CrO_3, and Al_2O_3 layers, the static WCA measurement was performed using the sessile drop method. Three droplets of Milli-Q water were placed randomly at different locations on each sample. The projected images of the droplets, after having been settled on the substrates with no noticeable change in their shapes, were analyzed for determining contact angles.

2.6. Cell Culture. Human bone marrow-derived mesenchymal stem cells (Lonza) were used for the cell experiments. The growth medium consisted of Alpha modified Eagle medium (Gibco), 10% (v/v) fetal bovine serum (Gibco), and 0.1% (v/v) ascorbic acid 2-phosphate (Sigma). Cells were incubated at 37 °C, 5% CO_2. The cells were harvested at approximately 80−90% confluency from T75 culture flasks by trypsin for 3−5 min at 37 °C for further subcultures.

2.7. Cell Adhesion Studies. All circular samples (Ø14 mm) were treated with 70% ethanol for sterilization and placed in 24-wells microtiter plates overnight. Afterward, hBM-MSCs were seeded onto the samples in 24-well plates at a density of 1×10^4 cells/well for cell adhesion. All plates were stored in an incubator at 37 °C and 5% CO_2 for 2 days. The hBM-MSCs were fixated with 3.7% paraformaldehyde (Sigma-Aldrich) in PBS for 20 min at room temperature and subsequently washed 3 times with PBS. Afterwards, the cell membrane was permeabilized with 0.5% TritonX-100 (Sigma-Aldrich) solution for 3 min. A 5% BSA in PBS solution was added for 30 min to block nonspecific binding. After withdrawing the BSA solution, the primary antibody against vinculin (clone hVin-1, Sigma, 1:100) was used in combination with a secondary FITC-labeled goat-antimouse antibody (Jackson Immunolab, 1:100). In addition, DAPI and TRITC-phalloidin were used to stain the cell nuclei and F-actin, respectively. Cells were observed using a LEICA TCS SP2 CLSM equipped with a 40× NA 0.80 water immersion objective. Additionally, the nuclei and F-actin were observed using TissueFaxs, with a Zeiss AxioImager Z1Microscope System (Tissue-Gnostics GmbH, Vienna, Austria) at 10× magnification. The complete samples were scanned, and images acquired together using the Tissue-Gnostics software. Image analysis of focal adhesion images acquired with CLSM was done by using Focal Adhesion Analysis Server,[41] and ImageJ software was used to measure the cell surface coverage, area, orientation, and elongation. Cell surface coverage was calculated by dividing the total surface area by the area of F-actin. Cell orientation was defined as the angle between the major axis of the ellipse and the direction of wrinkles. Cell elongation was quantified as the aspect ratio between the cell length and width measured on the fluorescent F-actin stained cells. Therefore, the aspect ratio of a circle cell is one.

2.8. Statistical Analysis. All data points are expressed as mean values ± standard deviation. Statistical analysis was performed using Origin 9.0 software. All data were analyzed using one way analysis of variance (ANOVA) with Tukey's test to determine differences between groups. A value of $p < 0.05$ was considered to be statistically significant.

3. RESULTS

3.1. Inorganic Aligned Topography Gradient Formation. The topographical gradient fabrication process for SiO_2 and metal oxides is illustrated in Figure 1. PDMS is

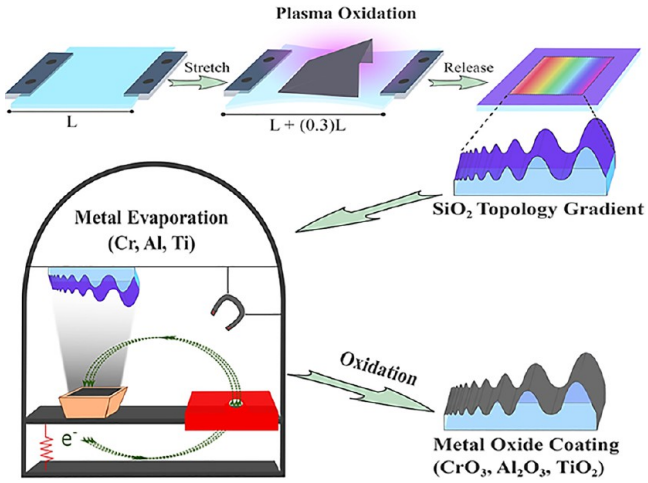

Figure 1. Schematic illustration of the process to prepare wrinkled gradients with SiO_2 via prolonged plasma oxidation and different metal oxide coatings by metal evaporation and exposure to air under ambient conditions.

uniaxially stretched (30% elongation) and plasma oxidized shielding the surface with a right angled triangular prism mask. Different oxidation parameters are used to control the final features (method 1:100 s plasma treating time, 45° mask angle, 60 mTorr stable pressure; method 2:650 s plasma treating time, 30° mask angle, 25 mTorr stable pressure). Releasing the strain, a stable wrinkled topographic gradient is generated which is tunable as a function of plasma treating time, mask angle, and operating pressure.[25,42] It has to be noted that all wrinkle samples were postoxidized with air plasma for 10 min to exclude any chemical or stiffness variations and provide a bioglass-like (SiO_2) top layer. Finally, we deposit different metal films of 10−15 nm thickness (Ti, Cr, and Al) on PDMS wrinkled gradients by metal evaporation, which resulted in the metal oxides after exposure to air (more information found in the Methods section).

The topography gradients were investigated using AFM. Metal evaporation did not alter the wrinkle features (Figure 2). However, more cracks were observed on the nanowrinkle gradient with metal coating as compared to the oxidized PDMS gradient surface, probably because of the metal residual stress.[43] Measurements were acquired between 0 and 10 mm with 2 mm intervals. The wrinkle size increased from the least exposed side to the most exposed side (open side of the mask) for both oxidation times of 100 and 650 s. The unidirectional gradients were obtained in a highly reproducible manner with amplitudes ranging from 49 to 2561 nm and wavelengths between 464 and 7121 nm as shown in Figures 3A and B. Both amplitude and wavelength display a continuous gradual change. Importantly, Figures 3A and B shows that the topography after metal coating and oxidation was preserved. The topographical dimension range obtained in our study encompasses similar range of individual collagen fibers, varying in diameter from few

DOI: 10.1021/acsami.7b08237
ACS Appl. Mater. Interfaces 2017, 9, 31433−31445

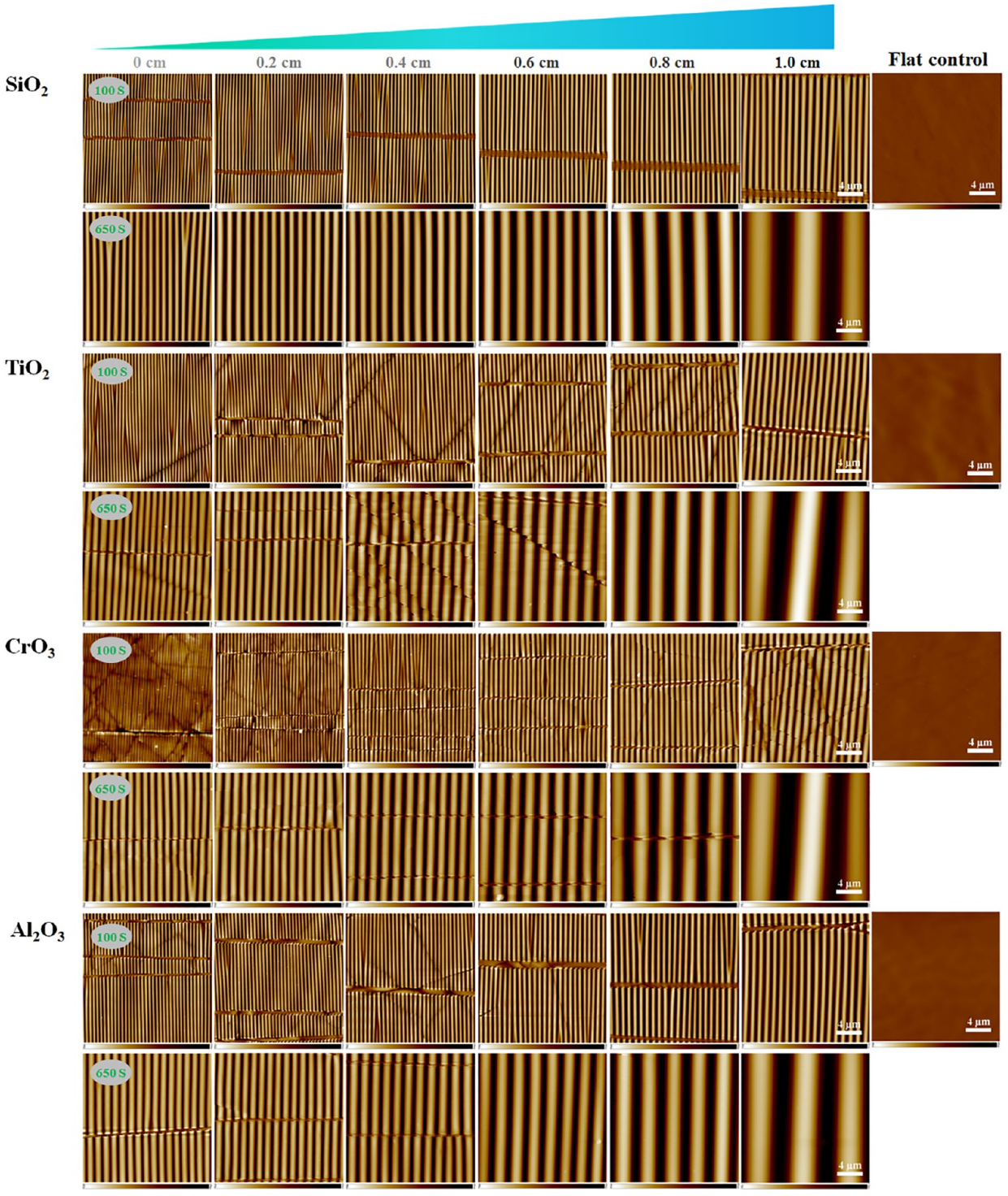

Figure 2. AFM images of topography (wrinkle) gradients with SiO_2 and the different metal oxide coatings along the 1.0 cm PDMS substrate. Scale bars are 4 μm and apply to all images. Also shown are flat substrates obtained under the same conditions only without applying unidirectional strain.

nanometers to ~150 nm within native ECM and collagen fiber bundles from several hundred nanometers to ~400 μm in diameter depending on the tissue type.[32,44,45]

To confirm the chemical composition of the surfaces, XPS measurements were carried out. Figure 3C shows the XPS spectra and confirmed overoxidized PDMS (SiO_2), TiO_2, CrO_3, and Al_2O_3 surface chemistry. The Ti peaks at binding energies of 459 and 465 eV are consistent with Ti^{4+}, confirming the presence of TiO_2 on the PDMS surface. The Cr peak at binding energy of 577 eV is consistent with Cr^{6+} in the corresponding oxide form, namely CrO_3. The Al peak at binding energy of 75 eV is consistent with Al^{3+}, confirming the presence of Al_2O_3.

Static WCA measurement before and after metal oxide layer generation on flat surfaces displayed similar wettability (94–102°) (Figure S1); no significant difference was detected on either metal oxide surfaces ($p > 0.05$). AFM test before and after metal oxide formation on flat surfaces showed similar Young's modulus (90–107 MPa) (Figure S2). Similar

DOI: 10.1021/acsami.7b08237
ACS Appl. Mater. Interfaces 2017, 9, 31433–31445

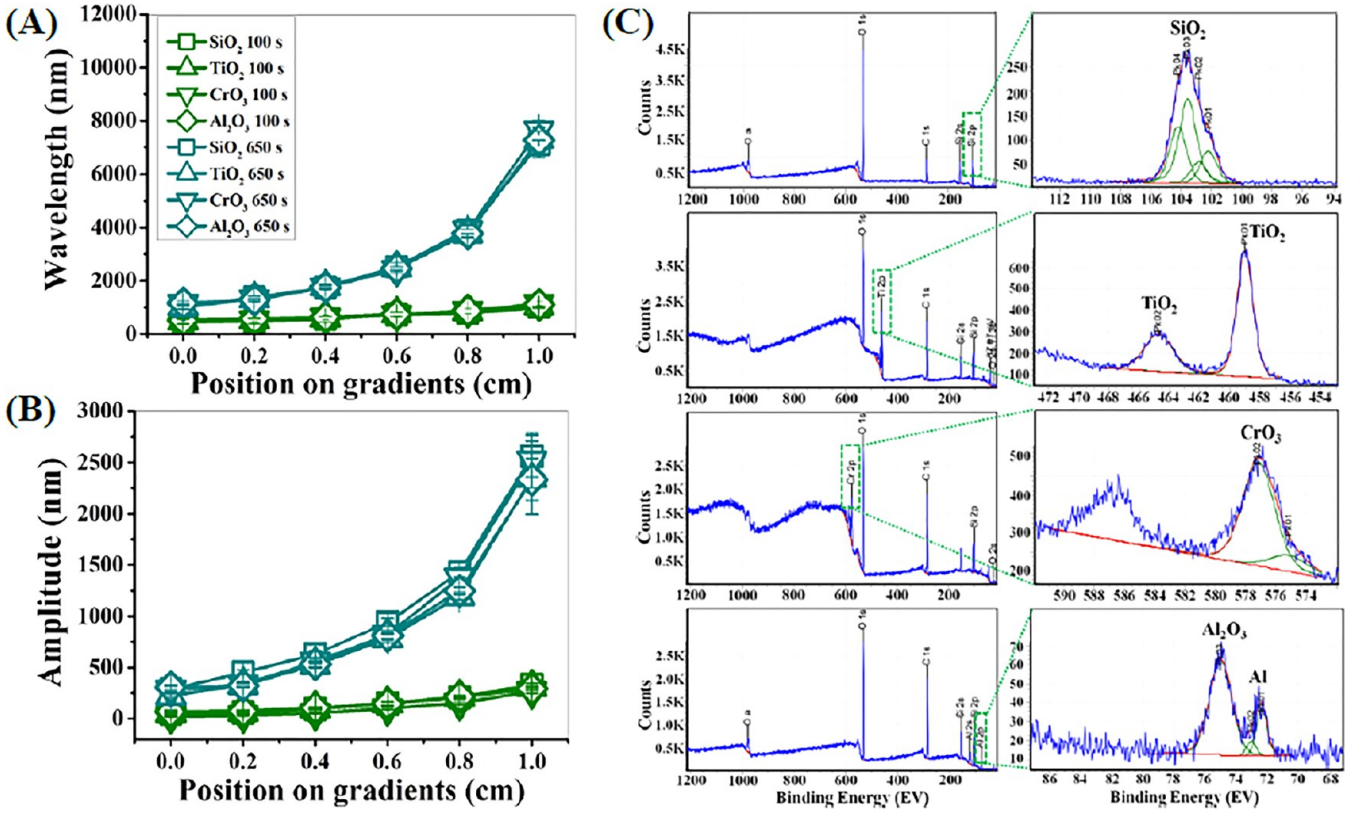

Figure 3. (A and B) Dependence of the wavelength and amplitude of created wrinkle gradients with different surface compositions. The 650s surfaces start where the 100s surfaces end with respect to wavelength and amplitude. Data are reported as mean ± standard deviation (SD) (n = 30 wrinkles). (C) XPS spectra of wrinkle gradients with SiO_2 and different metal oxide layers.

wettability and stiffness mean that any observed differences in cell behavior on the respective surfaces would, in fact, be due to topographical features and materials chemistry.

3.2. hBM-MSC Behavior on Inorganic Topographical Gradients. With our technology we designed a comprehensive material surface topography library that allows us to investigate which feature sizes yield optimal cell behavior. As a model cell type hBM-MSCs were used, as these cells isolated from human bone marrow are widely being employed as a promising source of cells for tissue engineering and regenerative medicine (TERM), owing to their potential to differentiate into a number of phenotypes, including adipocytes, chondrocytes, and osteocytes and production of trophic mediators.[46−48] Importantly, hBM-MSCs have previously been shown to be sensitive to surface properties[49] such as topography,[50] stiffness,[7,51] chemistry,[52] and wettability.[53]

To evaluate the viability of hBM-MSCs on SiO_2, TiO_2, CrO_3, and Al_2O_3 surfaces without a wrinkle feature, XTT viability assays were performed after 2 days of culture (Figure S2). Polystyrene tissue culture plates (TCP) were used as a positive control. Cells remained viable, and no significant difference was found on either surface ($p > 0.05$), which indicates that there were no cytotoxic effects derived from SiO_2 or the vapor-deposited metals TiO_2, CrO_3, and Al_2O_3. Furthermore, the fact that cell metabolic activity on SiO_2 and metal oxide interfaces was comparable to TCP control highlights the applicability of the interface design as a suitable surface treatment method for exploring cell−material interactions.

To study the response of hBM-MSCs toward the various wrinkled gradients, hBM-MSCs were seeded on these surfaces and allowed to attach and spread for 2 days, and the cell response to the mechanochemical cues was investigated. As shown in Figure 4, macroscopic cell behavior was observed by automated fluorescence microscopy imaging (TissueFAXS) in a high-throughput manner which enabled the observation of the surfaces as a whole with still the possibility of performing confocal laser scanning microscopy (CLSM). Cells on flat surfaces with different inorganic biomaterial interfaces are also shown in Figure 4 for comparison. The overview images on the TiO_2 gradients clearly display more cell surface coverage after two days than those of gradients with SiO_2 and other metal oxides. The result indicates that the cell surface coverage was affected by the materials chemistry. Another observation is that for the area with microscale wrinkles on TiO_2 gradient surfaces (i.e., range from the sixth (amplitude: 785 nm/wavelength: 2490 nm) to the seventh (amplitude: 1196 nm/wavelength: 3765 nm)) induces larger cell surface coverage than other areas. For the SiO_2 interface, cell surface coverage first decreases and then increases with increasing the wrinkle size. It suggests that cell spreading was affected by the topographic dimensions as well as materials chemistry. We observed from the actin-stained cell images that cells cultured on all substrates were highly elongated. Cell elongation increased with increasing wrinkle sizes. More elongation was observed on the Al_2O_3 interface as compared to the other interfaces. Therefore, cell elongation was affected synergistically by topographical dimension and material interface. In addition, we observed that cell alignment increased with increasing the wrinkle size on all interfaces. On all nanostructured surfaces ($^{0-1.0\ cm}100S_{grad}$, $^{0-0.4\ cm}650S_{grad}$ oxidation surfaces) independent of materials chemistry, limited cell alignment was observed. The $^{0.4-1.0\ cm}650S_{grad}$ oxidation areas (larger wrinkles features) had a better cell alignment as

DOI: 10.1021/acsami.7b08237
ACS Appl. Mater. Interfaces 2017, 9, 31433−31445

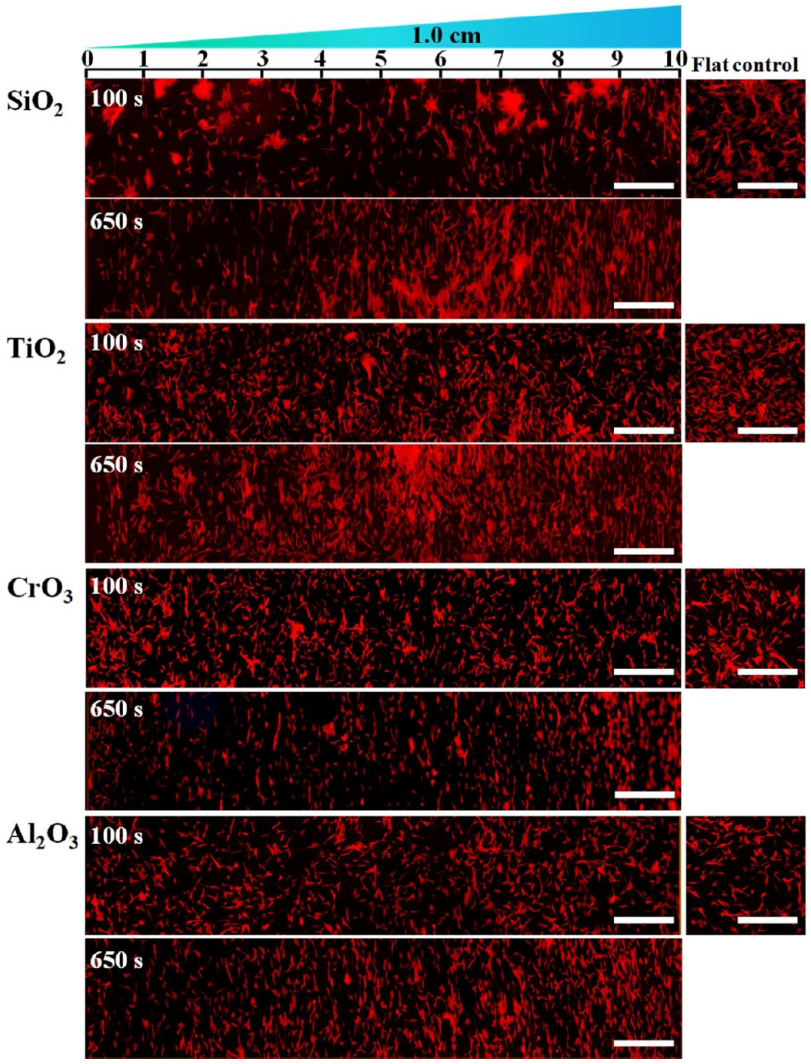

Figure 4. Fluorescence microscopy images of slices of the gradients are shown representing the full length of the samples for the gradients (scale bars = 1 mm). The red color is for TRITC−phalloidin.

compared to the areas with smaller wrinkle features. In particular, $^{0.9-1.0\ cm}650S_{grad}$ oxidation surfaces had an excellent cell alignment. Therefore, cell alignment is significantly affected depending on topographical dimensions. Importantly, these platforms enable defining the threshold of wrinkle features to induce cell elongation and alignment because engineering the precise structure is essential for the function of the cell and tissue.[54] Cell elongation and orientation is a morphological feature essential for many anisotropic tissue functions.[55]

For a better understanding of cell behavior on different gradients, material surface coverage, cell area, alignment, and elongation were determined by a quantitative analysis of the positively stained cells using ImageJ software (Figure 5). Figure 5A shows that cell surface coverage on wrinkle gradients with SiO_2, TiO_2, and CrO_3 first decreases and then increases with increasing the wrinkle size. There were no significant differences on wrinkle gradients with Al_2O_3. They indicate that cell surface coverage depends on both topographical dimension and materials chemistry. Figure 5B displays that the cell area on the wrinkle gradients for SiO_2 first decreases and then increases with increasing wrinkle size. There were no significant differences on wrinkle gradients for TiO_2, CrO_3, and Al_2O_3, which indicates that the cell area was unaffected by the topography dimension when combined with those interfaces. Topography combined with SiO_2 does affect the cell area, illustrating the delicate interplay between materials chemistry and topography parameters.

Cell alignment was stimulated significantly with increasing wrinkle size on all interfaces ($p < 0.05$), indicated by an angle closer to 0° (Figure 5C). Even for the nanopatterned surfaces ($^{0-1.0\ cm}100S_{grad}$), all biomaterial gradients promoted cell alignment compared to the flat controls (~45°) ($p < 0.05$). On micropatterned surfaces ($^{1.0\ cm}650S_{grad}$), average cell orientation angle reached ~10°. However, there are no significant differences between the different interface materials, indicating that cell alignment is mainly affected by the topography and not materials chemistry. Furthermore, the results suggest that an ideal range for topography-induced alignment exists in the wrinkles with 1.4−2.6 μm amplitude and 4.0−7.1 μm wavelength.

The degree of cell elongation provides further indication of cellular structural maturity and function expression.[56,57] Although orientation effects are material independent, elongation is affected by the materials chemistry. Figure 5D shows that cell elongation on wrinkle gradients with SiO_2, TiO_2, and Al_2O_3 increased with increasing the wrinkle size,

DOI: 10.1021/acsami.7b08237
ACS Appl. Mater. Interfaces 2017, 9, 31433−31445

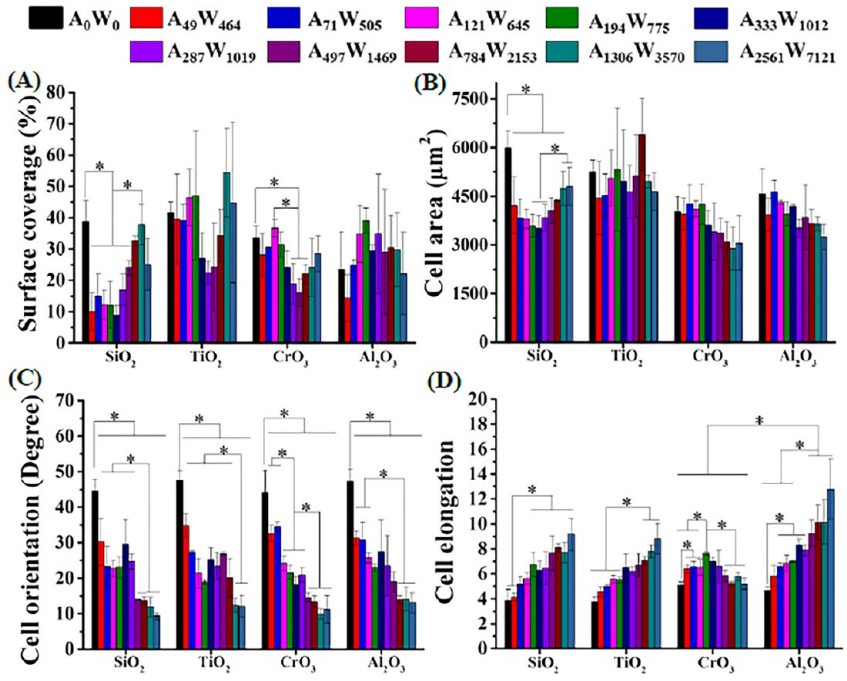

Figure 5. Macroscopic response of cells toward surface gradients with different interface materials. (A) Surface coverage by cells. (B) Cell area. (C) Cell orientation. (D) Cell elongation. (n = ∼150 cells). * indicates that both groups are statistically different ($p < 0.05$). A_0W_0 (amplitude 0 nm; wavelength 0 nm).

while on CrO_3 gradients, elongation first increases and then decreases with increasing the wrinkle size. Additionally, for Al_2O_3, topography and materials chemistry are synergistic, as the largest elongation (12.8 ± 2.4) was observed when topographic dimensions were maximized. The cell elongation may be an inherent property of a specific cell type (hBM-MSCs). However, we show that it depends also on the cell substratum interaction and that both topography and materials chemistry influence the elongation.

From confocal microscopy images (Figure S3), cell alignment and elongation can be observed more clearly. In addition to modulating cell morphology and cell alignment, phalloidin staining of the cytoskeleton (filamentous actin; F-actin) showed that hBM-MSCs cultured on the microtopography exhibited the highly elongated alignment of actin filaments along the surface patterns. In contrast, hBM-MSCs on either the flat or nanotopography did not display such an extended, aligned-actin morphology. Figure S4 allows us to observe high contrast images for F-actin arrangement and direction, displaying the alignment of cellular F-actin increasing with increasing the wrinkle size from nanometer to micrometer dimensions. F-actin presented a perfectly aligned cytoskeletal morphogenesis along wrinkle direction on the $^{1.0\ cm}650S_{grad}$ position. In comparison, the cells cultured onto flat and nanotopographies displayed a disordered cytoskeleton organization (Figure S4). This finding may also be attributed to wrinkle size that provide potential contact cues for F-actin.

Individual cells also frequently exhibited distinct organization of membrane protrusions (Figure S3). Depending on the local topography and materials chemistry, especially long/parallel filopodia were observed on the $^{0.5-1.0\ cm}650S_{Grad}$ of TiO_2, Al_2O_3, and CrO_3 interfaces. Surprisingly, we found that a higher amount of filopodia was typically observed on the microtopography. These filopodia on such a dimension were also longer than those on the flat or nanotopography gradient substrates. These results suggest that oriented cell outgrowth on the wrinkle substrate might be the result of a sensing mechanism performed by filopodia, because they are the organelles that work as sensors.[15,58,59] In addition, hBM-MSCs filopodia around the cells on microtopography can enhance cell−cell interactions by increasing direct contact with neighboring cells, even if they are far away.

In addition, the formation of focal adhesion contacts was analyzed using immunofluorescent staining for vinculin and visualized by CLSM. Major differences in focal adhesion number and morphology as well as orientation were observed. For SiO_2 interfaces, on the flat control and $^{0-0.5\ cm}100S_{Grad}$ surfaces, hBM-MSCs had more well-defined dash-like vinculin spots (typical for mature focal adhesions) compared to the dot-like (transient) vinculin spots found for hBM-MSCs cultured on the $^{0.75-1.0\ cm}100S_{Grad}$ and $^{0-1.0\ cm}650S_{Grad}$ surfaces. Furthermore, focal adhesion points decreased with increasing the wrinkle size. On TiO_2, CrO_3, and Al_2O_3 interfaces, there are many mature focal adhesions found on all surfaces. In contrast, there are more focal adhesions at the TiO_2 interface than at the others, and focal adhesion points decreased with increasing the wrinkle size on flat, $^{0-1.0\ cm}100S_{Grad}$, and $^{0-0.5\ cm}650S_{Grad}$ surfaces. Interestingly, focal adhesions in cells plated on microtopographical surfaces ($^{0.75-1.0\ cm}650S_{Grad}$) became more numerous and elongated and oriented themselves along the major cell axis, coaligned with stress fibers, whereas cells plated on nanotopographical substrates formed less numerous and radially oriented adhesions. A closer observation of the focal adhesions as presented in Figure 6 revealed that many cells on the microtopography that had high elongation and alignment contained elongated and uniformly oriented focal adhesions. This observation raises the notion that focal adhesion alignment may precede cell elongation and determine the direction of the future elongation axis. These data also indicate that topographical dimension and materials chemistry can

DOI: 10.1021/acsami.7b08237
ACS Appl. Mater. Interfaces 2017, 9, 31433−31445

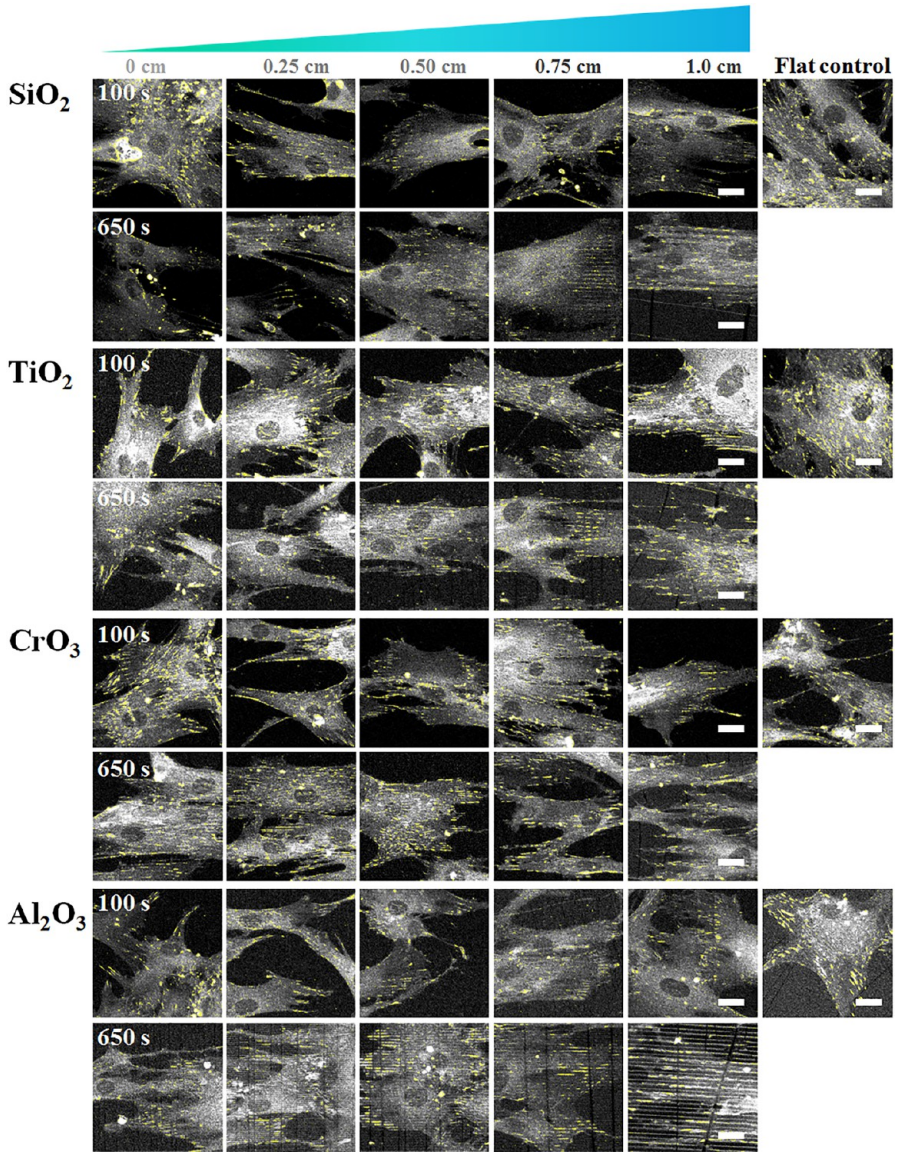

Figure 6. Highlighted focal adhesion contact points for hBM-MSCs after two days cultivation on wrinkle gradient surfaces with different interface biomaterials. Scale bars are 22 μm and apply to all images.

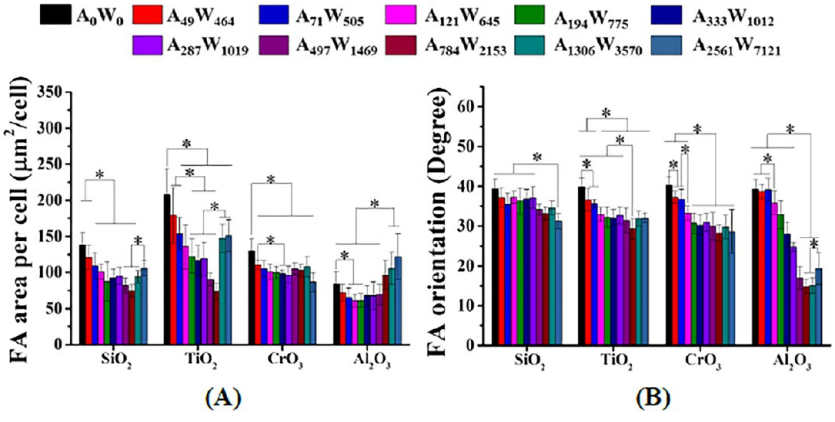

Figure 7. Dependence of focal adhesion area per cell (A) and focal adhesion orientation (B) on wrinkle gradients with different interface materials, respectively. Data are reported as mean ± standard deviation (SD) (n = ~100 cells). * indicates that both groups are statistically different ($p < 0.05$). A_0W_0 (amplitude 0 nm; wavelength 0 nm).

DOI: 10.1021/acsami.7b08237
ACS Appl. Mater. Interfaces 2017, 9, 31433−31445

provide synergistic stimulation to affect formation and organization of focal adhesion complexes. Most likely, focal adhesions are herein the sensors that allow us to interpret the wrinkle pattern cues.[60] Notably, we found an apparent correlation between focal adhesion orientation to cell alignment.

To better understand the focal adhesion behavior on different gradients, focal adhesion area per cell (FA area/cell; μm^2/cell) and FA orientation were determined by a quantitative analysis of the positively stained focal adhesions (Figure 7). FAs play a central role in delegating extracellular mechanical cues into cellular responses and in transferring contractile forces to the ECM. It has been demonstrated that FA area plays a critical role in cell adhesion, migration, and functions or differentiation and is therefore an insightful parameter to study. Surprisingly, for SiO_2, TiO_2, and Al_2O_3 interfaces, the trend of FA area per cell first decreases and then increases with increasing the wrinkle size. For CrO_3 interface, FA area per cell decreases only minor with increasing the wrinkle size on $^{0-1.0\ cm}100S_{Grad}$ nanowrinkle surface and remains constant on $^{0-1.0\ cm}650S_{Grad}$ microwrinkle surface. These results suggest that FA area per cell of hBM-MSCs is highly sensitive to the topographical gradient, especially on SiO_2, TiO_2, and Al_2O_3 interfaces. The optimal wrinkle dimensions selected here for different interfacial materials to promote FA formation are flat surfaces for SiO_2, TiO_2, and CrO_3 interfaces and wrinkle size (wavelength: 7121 nm; amplitude: 2561 nm) for Al_2O_3 surface.

For the SiO_2 interfaces, the FAs on microwrinkles become more oriented than those on flat and nanowrinkled surfaces, but not substantially. For TiO_2 and CrO_3 interfaces, the FA aligned more with the wrinkles when increasing from nano- to microtopographies; the effect is also not large here. However, on Al_2O_3 gradients, the effect was much more pronounced, and the FA initially oriented more with increasing wrinkle size, and then orientation diminished again. Therefore, the optimal wrinkle dimensions selected here for different interfacial materials to promote FA orientation are wrinkle size (wavelength: 7121 nm; amplitude: 2561 nm) for SiO_2 surface, wrinkle size range (wavelength: 732−7121 nm; amplitude: 146−2561 nm) for TiO_2 and CrO_3 surfaces, and wrinkle size range (wavelength: 1281−3776 nm; amplitude: 323−1248 nm) for Al_2O_3 surface.

4. DISCUSSION

Material properties (e.g., composition, topography, elasticity, or (bio)chemical signals) contribute significantly to governing the fate of cells.[7,49−51] The gradient platform system developed herein enables vast reduction of experimental efforts that would generally need numerous individual substrates of discrete inorganic biomaterial topography and chemical composition. In addition, cell behavior on our gradient surfaces was observed by automated fluorescence microscopy (TissueFAXS) in a high-throughput manner, which enabled the observation of the surfaces as a whole. Cell responses could be determined by a quantitative analysis of the positively stained cells using the high-throughput analysis technique (e.g., Tissue Quest software). We found that biomaterials chemistry combined with topographical cues make a significant combined contribution. The strategy of using gradients enables us to identify optimum combined surface parameters and screen efficiently whether costly engineering approaches for manufacturing inorganic biomaterials with specific surface parameters are worth the efforts. For the first time, biomimetic topographical gradients of various clinically relevant inorganic biomaterial interfaces were developed by using simple methods to study hBM-MSCs responses in vitro. Previously, gradients or chips on silicon wafers have been developed using photolithography for the use of polymer imprinting (e.g., polyurethane acrylate, polylactic acid, polystyrene) which were used for high-throughput screening of cell behavior.[27,31,61] Additionally, the evaporation approach on PDMS allows many variations in topography as PDMS can be easily patterned with various imprinting lithography approaches, enabling other structures to be assessed as well.

We found that an ideal range for topography-induced alignment exists in the micrometer range (Figures 1 and 2). However, ultrastructural analysis of the native ECM in anisotropic tissues indicates aligned collagen fibrils varying in diameter from a few nanometers to ∼150 nm and actual collagen fiber bundles from several hundred nanometers to ∼400 μm in diameter.[32,44,45] In comparison, in vitro results reveal that larger topographical dimensions (micrometer range) are required to promote cell orientation and maturation than cells would likely be exposed to in vivo. This disparity is likely attributable to three reasons: (1) materials chemistry, (2) the inherent differences in 3D and 2D cellular environments, and (3) cells directly interacting with fibril bundles. For materials chemistry (1), it is well-known that the basic building block of the extracellular matrix in native tissue is collagen. Cells prefer to adhere more to collagen than to inorganic biomaterials. Furthermore, this difference can likely be attributed to the differences between 3D and 2D microenvironments (2). In human anisotropic tissues, cells reside in a complex 3D microenvironment with cell-to-ECM and cell-to-cell interactions. Cells growing in 3D matrixes are surrounded and pressed by ECM fibers and other oriented cells. They could likely be more receptive to the uniformly surrounding topographical and mechanical cues. However, cells grown on 2D surfaces are influenced only by topographical signals at their basal surface. Consequently, cells on 2D surfaces would probably need more pronounced topographical stimuli to guide their uniaxial arrangement. Or, in case of direct fibril interaction (3), this can easily be understood because cells directly interact with microscale topographical cues of fibril bundles, which is in agreement with our results. In addition, it has been reported that the width of aligned microtopographical patterns strongly affected cultured cell bodies, therefore forcing them to align, grow, and move along the patterned trenches due to the restriction of space.[11,62] The "width" of a single cell body is one order of magnitude larger than that of the microwrinkle used in our study. Such anisotropic topographical dimensions can also induce cell alignment along the wrinkle direction. Probably, anisotropic topographies do not directly interact with the cell body. Instead, they interact with subcellular structures, including filopodia, focal adhesions, and subsequently F-actin (cytoskeleton). By a HTS for assessment of different aspects of cell behavior, we found a positive correlation of cell alignment with respect to the formation and orientation of the cytoskeleton, filopodia, and focal adhesions. It has been extensively documented that focal adhesions not only work like biochemical signal transducers but also act as mechanical sensors.[60] Furthermore, the size of focal adhesions is on the microscale.[63] On the basis of the observations in our study, we found that the establishment and organization of focal

DOI: 10.1021/acsami.7b08237
ACS Appl. Mater. Interfaces 2017, 9, 31433−31445

adhesions was clearly influenced by anisotropic wrinkles with different dimensions.

Meanwhile, materials chemistry also plays an important role in hBM-MSC behavior on otherwise identical micro/nano-wrinkle gradients. Cell spreading and adhesion are important cellular events modulating cell behavior. Our data suggests that although the same wrinkle gradients were used across our study, when interface materials are altered, there are significant differences found for cell responses. The findings show that both topography and interface material of the substrate can have a synergistic effect on interactions between stem cells and their ECM, influencing cell material surface coverage, elongation and orientation, the organization of the cytoskeleton, filopodia generation, as well as the formation and orientation of focal adhesion. Monitoring these processes indicated that cell elongation and alignment is preceded by the alignment of focal adhesions. Therefore, it is necessary to employ a high-throughput screening to evaluate optimum conditions for both existing and new biomaterials on the cell–material interface.

The practical application of HTS technology is expected to accelerate the clinical translation of inorganic biomaterials. Here, our wrinkled gradient platform with different interface materials can directly output the optimal wrinkle size for cell responses in an HTS manner. For instance, we can maximize cell surface coverage or adhesion on different inorganic biomaterials by tailoring material surface topographical dimension (Figure 4), which provides the important information for accelerating tissue repair and regeneration because it still remains a huge challenge due to lack of surface cell recognition sites. Cytoskeleton rearrangement and elongation play a key role in generating the signal transduction for changes in gene expression profile and cell trans-differentiation because the mechanical tension is transmitted to the nucleus through actin filament, and mechanotransduction can rearrange the centromere through deformation of the nucleus.[64,65] As reported, when human mesenchymal stem cells (hMSCs) are aligned better and elongated more due to the direct impact of the topographical size or pattern, osteogenic differentiation is enhanced,[66,67] which is of high importance particularly for orthopedic implants. In addition, Evelyn et al. reported that aligned and elongated hMSCs along the directional topography showed more neuronal markers (microtubule-associated protein 2 (MAP2)) compared to the flat control.[68] The incorporation of topography and chemical cues (retinoic acid) further promoted the up-regulation of MAP2; however, topography provided a stronger effect compared to retinoic acid alone on the flat surface. Chor et al. showed that hMSCs were coerced to align and elongate on a micropatterned fibronectin–PLGA surface, enhancing the up-regulation of genes related with neurogenesis and myogenesis even in the absence of any differentiation factors.[69] Therefore, topography-induced hMSC differentiation occurs through mechanotransduction, which is a very effective strategy to govern cell phenotype. With our HTS approach, we found that surface topography has a significant effect on the degree of cell alignment and elongation in an HTS manner (Figures 1 and 2). Cell alignment increases with increasing the wrinkle size, and the optimal wrinkle dimension for promoting hBM-MSCs alignment was identified using the HTS platform. Further, the signals from the underlying topography are transduced through the FAs to the actin cytoskeleton before deforming the nucleus to affect cellular gene expression and phenotype. Osteogenic differentiation is more prevalent in MSCs with more focal adhesions.[70] We also defined the optimal wrinkle dimensions for different inorganic biomaterials to promote FA formation (Figures 6 and 7). The platform developed herein can be used with various cell types but can also focus on cell function correlated to tissues with known intrinsic anisotropy (e.g., skeletal muscle, blood vessels, neurons, etc.) to screen for optimal conditions. As topography and materials composition influence cell behavior, optimum interactions for cell growth and tissue response can be identified and used to enhance, e.g., orthopedic implants (e.g., tendon-to-implant attachment also relying intrinsic directionality and stimulation of bone and osteochondral tissue). This is particularly interesting for tissues relying on intrinsic directionality such as muscle, tendon, and blood vessels. To achieve efficiency and complexity, high-throughput approaches are excellent tools toward establishing property–activity relationships between biointerfaces and biological systems. The combination of a novel HTS approach, advanced imaging, and efficient analysis methods is positioned to accelerate the pace of discovery for next-generation materials for biotechnology and medicine.

5. CONCLUSIONS

For the first time, biomimetic topographical gradients of various clinically relevant inorganic biomaterial interfaces were developed via combination of masked plasma oxidation and metal deposition oxidation methods to study hBM-MSC responses in vitro. It is found that certain features of hBM-MSC behaviors (cell surface coverage, area, and focal adhesions) on different interface materials are worse than those on the flat and microstructured surfaces. The optimal wrinkle dimension selected here (wavelength: 7121 nm; amplitude: 2561 nm) for promoting hBM-MSC alignment, cytoskeleton arrangement, long/parallel filopodia, and focal adhesion assembly and orientation was obtained based on the above platforms. The gradient platforms containing both wrinkles and materials chemistry can generate synergistic effects on the response of hBM-MSCs, indicating that we need to apply a screening to assess optimum conditions for both current and new biomaterials. This versatile platform system employed herein provides a novel strategy to better understand the structure–function relationships between surface properties and biological performance that would accelerate the development of desired biomedical implants and tissue engineering scaffolds.

■ ASSOCIATED CONTENT

Supporting Information

The Supporting Information is available free of charge on the ACS Publications website at DOI: 10.1021/acsami.7b08237.

Physical surface characterization using water contact angle, atomic force microscopy for Young's modulus determination, cell viability, and laser scanning confocal microscopy images used for focal adhesion behavior (PDF)

■ AUTHOR INFORMATION

Corresponding Author

*E-mail: p.van.rijn@umcg.nl; Phone: +31-50 361 6066.

ORCID

Qihui Zhou: 0000-0003-2474-4197

Patrick van Rijn: 0000-0002-2208-5725

DOI: 10.1021/acsami.7b08237
ACS Appl. Mater. Interfaces 2017, 9, 31433–31445

Notes

The authors declare no competing financial interest.

■ ACKNOWLEDGMENTS

Q.H.Z. is very grateful for financial support from the China Scholarship Council (Grant 201406630003). Part of the work was performed in the UMCG Microscopy and Imaging Center (UMIC), sponsored by NWO Grant 40-00506-98-9021. Joop de Vries is gratefully acknowledged for help with AFM, XPS, and plasma system maintenance. Klaas Sjollema is kindly acknowledged for help with TissueFaxs microscopy and Imaris software.

■ REFERENCES

(1) Tzima, E.; Irani-Tehrani, M.; Kiosses, W. B.; Dejana, E.; Schultz, D. A.; Engelhardt, B.; Cao, G.; DeLisser, H.; Schwartz, M. A. A Mechanosensory Complex That Mediates the Endothelial Cell Response to Fluid Shear Stress. *Nature* **2005**, *437* (7057), 426−431.

(2) Discher, D. E.; Janmey, P.; Wang, Y.-L. Tissue Cells Feel and Respond to the Stiffness of Their Substrate. *Science* **2005**, *310* (5751), 1139−1143.

(3) Bettinger, C. J.; Langer, R.; Borenstein, J. T. Engineering Substrate Topography at the Micro- and Nanoscale to Control Cell Function. *Angew. Chem., Int. Ed.* **2009**, *48* (30), 5406−5415.

(4) Mei, Y.; Saha, K.; Bogatyrev, S. R.; Yang, J.; Hook, A. L.; Kalcioglu, Z. I.; Cho, S.-W.; Mitalipova, M.; Pyzocha, N.; Rojas, F.; Van Vliet, K. J.; Davies, M. C.; Alexander, M. R.; Langer, R.; Jaenisch, R.; Anderson, D. G. Combinatorial Development of Biomaterials for Clonal Growth of Human Pluripotent Stem Cells. *Nat. Mater.* **2010**, *9* (9), 768−778.

(5) Shin, H.; Jo, S.; Mikos, A. G. Biomimetic Materials for Tissue Engineering. *Biomaterials* **2003**, *24* (24), 4353−4364.

(6) Flaim, C. J.; Teng, D.; Chien, S.; Bhatia, S. N. Combinatorial Signaling Microenvironments for Studying Stem Cell Fate. *Stem Cells Dev.* **2008**, *17* (1), 29−40.

(7) Mao, A. S.; Shin, J.-W.; Mooney, D. J. Effects of Substrate Stiffness and Cell-Cell Contact on Mesenchymal Stem Cell Differentiation. *Biomaterials* **2016**, *98*, 184−191.

(8) Teo, B. K. K.; Wong, S. T.; Lim, C. K.; Kung, T. Y. S.; Yap, C. H.; Ramagopal, Y.; Romer, L. H.; Yim, E. K. F. Nanotopography Modulates Mechanotransduction of Stem Cells and Induces Differentiation through Focal Adhesion Kinase. *ACS Nano* **2013**, *7* (6), 4785−4798.

(9) Dalby, M. J.; Gadegaard, N.; Oreffo, R. O. C. Harnessing Nanotopography and Integrin-Matrix Interactions to Influence Stem Cell Fate. *Nat. Mater.* **2014**, *13* (6), 558−569.

(10) Yang, J.; Rose, F. R. A. J.; Gadegaard, N.; Alexander, M. R. A High-Throughput Assay of Cell-Surface Interactions Using Topographical and Chemical Gradients. *Adv. Mater.* **2009**, *21* (3), 300−304.

(11) Kapoor, A.; Caporali, E. H. G.; Kenis, P. J. A.; Stewart, M. C. Microtopographically Patterned Surfaces Promote the Alignment of Tenocytes and Extracellular Collagen. *Acta Biomater.* **2010**, *6* (7), 2580−2589.

(12) Lauria, I.; Kramer, M.; Schröder, T.; Kant, S.; Hausmann, A.; Böke, F.; Leube, R.; Telle, R.; Fischer, H. Inkjet Printed Periodical Micropatterns Made of Inert Alumina Ceramics Induce Contact Guidance and Stimulate Osteogenic Differentiation of Mesenchymal Stromal Cells. *Acta Biomater.* **2016**, *44*, 85−96.

(13) McNamara, L. E.; McMurray, R. J.; Biggs, M. J. P.; Kantawong, F.; Oreffo, R. O. C.; Dalby, M. J. Nanotopographical Control of Stem Cell Differentiation. *J. Tissue Eng.* **2010**, *1* (1), 120623.

(14) Dolatshahi-Pirouz, A.; Jensen, T.; Kraft, D. C.; Foss, M.; Kingshott, P.; Hansen, J. L.; Larsen, A. N.; Chevallier, J.; Besenbacher, F. Fibronectin Adsorption, Cell Adhesion, and Proliferation on Nanostructured Tantalum Surfaces. *ACS Nano* **2010**, *4* (5), 2874−2882.

(15) Albuschies, J.; Vogel, V. The Role of Filopodia in the Recognition of Nanotopographies. *Sci. Rep.* **2013**, *3*, 1658.

(16) Bae, W.-G.; Kim, J.; Choung, Y.-H.; Chung, Y.; Suh, K. Y.; Pang, C.; Chung, J. H.; Jeong, H. E. Bio-Inspired Configurable Multiscale Extracellular Matrix-like Structures for Functional Alignment and Guided Orientation of Cells. *Biomaterials* **2015**, *69*, 158−164.

(17) Stevens, M. M.; George, J. H. Exploring and Engineering the Cell Surface Interface. *Science* **2005**, *310* (5751), 1135−1138.

(18) Wegst, U. G. K.; Bai, H.; Saiz, E.; Tomsia, A. P.; Ritchie, R. O. Bioinspired Structural Materials. *Nat. Mater.* **2014**, *14* (1), 23−36.

(19) Yin, Z.; Chen, X.; Chen, J. L.; Shen, W. L.; Nguyen, T. M. H.; Gao, L.; Ouyang, H. W. The Regulation of Tendon Stem Cell Differentiation by the Alignment of Nanofibers. *Biomaterials* **2010**, *31* (8), 2163−2175.

(20) Engelmayr, G. C.; Cheng, M.; Bettinger, C. J.; Borenstein, J. T.; Langer, R.; Freed, L. E. Accordion-like Honeycombs for Tissue Engineering of Cardiac Anisotropy. *Nat. Mater.* **2008**, *7* (12), 1003−1010.

(21) Georgiou, M.; Bunting, S. C. J.; Davies, H. A.; Loughlin, A. J.; Golding, J. P.; Phillips, J. B. Engineered Neural Tissue for Peripheral Nerve Repair. *Biomaterials* **2013**, *34* (30), 7335−7343.

(22) Zhou, Q.; Wünnemann, P.; Kühn, P. T.; de Vries, J.; Helmin, M.; Böker, A.; van Kooten, T. G.; van Rijn, P. Mechanical Properties of Aligned Nanotopologies for Directing Cellular Behavior. *Adv. Mater. Interfaces* **2016**, *3* (18), 1600275.

(23) Zhou, Q.; Xie, J.; Bao, M.; Yuan, H.; Ye, Z.; Lou, X.; Zhang, Y. Engineering Aligned Electrospun PLLA Microfibers with Nano-Porous Surface Nanotopography for Modulating the Responses of Vascular Smooth Muscle Cells. *J. Mater. Chem. B* **2015**, *3*, 4439−4450.

(24) Wang, Y.; Shi, H.; Qiao, J.; Tian, Y.; Wu, M.; Zhang, W.; Lin, Y.; Niu, Z.; Huang, Y. Electrospun Tubular Scaffold with Circumferentially Aligned Nanofibers for Regulating Smooth Muscle Cell Growth. *ACS Appl. Mater. Interfaces* **2014**, *6* (4), 2958−2962.

(25) Zhou, Q.; Kuhn, P. T.; Huisman, T.; Nieboer, E.; van Zwol, C.; van Kooten, T. G.; van Rijn, P. Directional Nanotopographic Gradients: A High-Throughput Screening Platform for Cell Contact Guidance. *Sci. Rep.* **2015**, *5*, 16240.

(26) Faia-Torres, A. B.; Guimond-Lischer, S.; Rottmar, M.; Charnley, M.; Goren, T.; Maniura-Weber, K.; Spencer, N. D.; Reis, R. L.; Textor, M.; Neves, N. M. Differential Regulation of Osteogenic Differentiation of Stem Cells on Surface Roughness Gradients. *Biomaterials* **2014**, *35* (33), 9023−9032.

(27) Kim, D.-H.; Han, K.; Gupta, K.; Kwon, K. W.; Suh, K.-Y.; Levchenko, A. Mechanosensitivity of Fibroblast Cell Shape and Movement to Anisotropic Substratum Topography Gradients. *Biomaterials* **2009**, *30* (29), 5433−5444.

(28) Kim, D.; Seo, C.; Han, K.; Kwon, K. W.; Levchenko, A.; Suh, K. Guided Cell Migration on Microtextured Substrates with Variable Local Density and Anisotropy. *Adv. Funct. Mater.* **2009**, *19* (10), 1579−1586.

(29) Khung, Y. L.; Barritt, G.; Voelcker, N. H. Using Continuous Porous Silicon Gradients to Study the Influence of Surface Topography on the Behaviour of Neuroblastoma Cells. *Exp. Cell Res.* **2008**, *314* (4), 789−800.

(30) Faia-Torres, A. B.; Charnley, M.; Goren, T.; Guimond-Lischer, S.; Rottmar, M.; Maniura-Weber, K.; Spencer, N. D.; Reis, R. L.; Textor, M.; Neves, N. M. Osteogenic Differentiation of Human Mesenchymal Stem Cells in the Absence of Osteogenic Supplements: A Surface-Roughness Gradient Study. *Acta Biomater.* **2015**, *28*, 64−75.

(31) Park, J.; Kim, D.-H.; Kim, H.-N.; Wang, C. J.; Kwak, M. K.; Hur, E.; Suh, K.-Y.; An, S. S.; Levchenko, A. Directed Migration of Cancer Cells Guided by the Graded Texture of the Underlying Matrix. *Nat. Mater.* **2016**, *15*, 792.

(32) Carson, D.; Hnilova, M.; Yang, X.; Nemeth, C. L.; Tsui, J. H.; Smith, A. S. T.; Jiao, A.; Regnier, M.; Murry, C. E.; Tamerler, C. Nanotopography-Induced Structural Anisotropy and Sarcomere Development in Human Cardiomyocytes Derived from Induced Pluripotent Stem Cells. *ACS Appl. Mater. Interfaces* **2016**, *8* (34), 21923−21932.

DOI: 10.1021/acsami.7b08237
ACS Appl. Mater. Interfaces 2017, 9, 31433−31445

(33) Webster, T. J.; Ergun, C.; Doremus, R. H.; Siegel, R. W.; Bizios, R. Enhanced Functions of Osteoblasts on Nanophase Ceramics. *Biomaterials* **2000**, *21* (17), 1803−1810.
(34) Roualdes, O.; Duclos, M.-E.; Gutknecht, D.; Frappart, L.; Chevalier, J.; Hartmann, D. J. In Vitro and in Vivo Evaluation of an Alumina−zirconia Composite for Arthroplasty Applications. *Biomaterials* **2010**, *31* (8), 2043−2054.
(35) Webster, T. J.; Siegel, R. W.; Bizios, R. Osteoblast Adhesion on Nanophase Ceramics. *Biomaterials* **1999**, *20* (13), 1221−1227.
(36) Webster, T. J.; Ergun, C.; Doremus, R. H.; Siegel, R. W.; Bizios, R. Specific Proteins Mediate Enhanced Osteoblast Adhesion on Nanophase Ceramics. *J. Biomed. Mater. Res.* **2000**, *51* (3), 475−483.
(37) Karlsson, M.; Pålsgård, E.; Wilshaw, P. R.; Di Silvio, L. Initial in Vitro Interaction of Osteoblasts with Nano-Porous Alumina. *Biomaterials* **2003**, *24* (18), 3039−3046.
(38) Wieland, M.; Textor, M.; Chehroudi, B.; Brunette, D. M. Synergistic Interaction of Topographic Features in the Production of Bone-like Nodules on Ti Surfaces by Rat Osteoblasts. *Biomaterials* **2005**, *26* (10), 1119−1130.
(39) Att, W.; Yamada, M.; Ogawa, T. Effect of Titanium Surface Characteristics on the Behavior and Function of Oral Fibroblasts. *Int. J. Oral Maxillofac. Implants* **2009**, *24* (3), 419−431.
(40) Tavangar, A.; Tan, B.; Venkatakrishnan, K. The Influence of Laser-Induced 3-D Titania Nanofibrous Platforms on Cell Behavior. *J. Biomed. Nanotechnol.* **2013**, *9* (11), 1837−1846.
(41) Berginski, M. E.; Gomez, S. M. The Focal Adhesion Analysis Server: A Web Tool for Analyzing Focal Adhesion Dynamics. *F1000Research* **2013**, *2*, 68.
(42) Bowden, N.; Huck, W. T. S.; Paul, K. E.; Whitesides, G. M. The Controlled Formation of Ordered, Sinusoidal Structures by Plasma Oxidation of an Elastomeric Polymer. *Appl. Phys. Lett.* **1999**, *75* (17), 2557−2559.
(43) Seghir, R.; Arscott, S. Controlled Mud-Crack Patterning and Self-Organized Cracking of Polydimethylsiloxane Elastomer Surfaces. *Sci. Rep.* **2015**, *5*, 14787.
(44) Ballester-Beltrán, J.; Biggs, M. J. P.; Dalby, M. J.; Salmerón-Sánchez, M.; Leal-Egaña, A. Sensing the Difference: The Influence of Anisotropic Cues on Cell Behavior. *Front. Mater.* **2015**, *2*, 39.
(45) Chaterji, S.; Kim, P.; Choe, S. H.; Tsui, J. H.; Lam, C. H.; Ho, D. S.; Baker, A. B.; Kim, D.-H. Synergistic Effects of Matrix Nanotopography and Stiffness on Vascular Smooth Muscle Cell Function. *Tissue Eng., Part A* **2014**, *20* (15−16), 2115−2126.
(46) Kern, S.; Eichler, H.; Stoeve, J.; Klüter, H.; Bieback, K. Comparative Analysis of Mesenchymal Stem Cells from Bone Marrow, Umbilical Cord Blood, or Adipose Tissue. *Stem Cells* **2006**, *24* (5), 1294−1301.
(47) Pittenger, M. F.; Mackay, A. M.; Beck, S. C.; Jaiswal, R. K.; Douglas, R.; Mosca, J. D.; Moorman, M. A.; Simonetti, D. W.; Craig, S.; Marshak, D. R. Multilineage Potential of Adult Human Mesenchymal Stem Cells. *Science* **1999**, *284* (5411), 143−147.
(48) Chamberlain, G.; Fox, J.; Ashton, B.; Middleton, J. Concise Review: Mesenchymal Stem Cells: Their Phenotype, Differentiation Capacity, Immunological Features, and Potential for Homing. *Stem Cells* **2007**, *25* (11), 2739−2749.
(49) Schaap-Oziemlak, A. M.; Kühn, P. T.; van Kooten, T. G.; van Rijn, P. Biomaterial−stem Cell Interactions and Their Impact on Stem Cell Response. *RSC Adv.* **2014**, *4* (95), 53307−53320.
(50) Dalby, M. J.; McCloy, D.; Robertson, M.; Wilkinson, C. D. W.; Oreffo, R. O. C. Osteoprogenitor Response to Defined Topographies with Nanoscale Depths. *Biomaterials* **2006**, *27* (8), 1306−1315.
(51) Chuah, Y. J.; Zhang, Y.; Wu, Y.; Menon, N. V.; Goh, G. H.; Lee, A. C.; Chan, V.; Zhang, Y.; Kang, Y. Combinatorial Effect of Substratum Properties on Mesenchymal Stem Cell Sheet Engineering and Subsequent Multi-Lineage Differentiation. *Acta Biomater.* **2015**, *23*, 52−62.
(52) Murphy, A. R.; John, P. S.; Kaplan, D. L. Modification of Silk Fibroin Using Diazonium Coupling Chemistry and the Effects on hMSC Proliferation and Differentiation. *Biomaterials* **2008**, *29* (19), 2829−2838.
(53) Kühn, P. T.; Zhou, Q.; van der Boon, T. A. B.; Schaap-Oziemlak, A. M.; van Kooten, T. G.; van Rijn, P. Double Linear Gradient Biointerfaces for Determining Two-Parameter Dependent Stem Cell Behavior. *ChemNanoMat* **2016**, *2* (5), 407−413.
(54) Dvir, T.; Timko, B. P.; Kohane, D. S.; Langer, R. Nanotechnological Strategies for Engineering Complex Tissues. *Nat. Nanotechnol.* **2011**, *6* (1), 13−22.
(55) Prager-Khoutorsky, M.; Lichtenstein, A.; Krishnan, R.; Rajendran, K.; Mayo, A.; Kam, Z.; Geiger, B.; Bershadsky, A. D. Fibroblast Polarization Is a Matrix-Rigidity-Dependent Process Controlled by Focal Adhesion Mechanosensing. *Nat. Cell Biol.* **2011**, *13* (12), 1457−1465.
(56) Relan, N. K.; Yang, Y.; Beqaj, S.; Miner, J. H.; Schuger, L. Cell Elongation Induces Laminin α2 Chain Expression in Mouse Embryonic Mesenchymal Cells Role in Visceral Myogenesis. *J. Cell Biol.* **1999**, *147* (6), 1341−1350.
(57) Au, H. T. H.; Cheng, I.; Chowdhury, M. F.; Radisic, M. Interactive Effects of Surface Topography and Pulsatile Electrical Field Stimulation on Orientation and Elongation of Fibroblasts and Cardiomyocytes. *Biomaterials* **2007**, *28* (29), 4277−4293.
(58) Chan, C. E.; Odde, D. J. Traction Dynamics of Filopodia on Compliant Substrates. *Science* **2008**, *322*, 1687−1691.
(59) Lim, J. Y.; Donahue, H. J. Cell Sensing and Response to Micro- and Nanostructured Surfaces Produced by Chemical and Topographic Patterning. *Tissue Eng.* **2007**, *13* (8), 1879−1891.
(60) Shemesh, T.; Geiger, B.; Bershadsky, A. D.; Kozlov, M. M. Focal Adhesions as Mechanosensors: A Physical Mechanism. *Proc. Natl. Acad. Sci. U. S. A.* **2005**, *102* (35), 12383−12388.
(61) Unadkat, H. V.; Hulsman, M.; Cornelissen, K.; Papenburg, B. J.; Truckenmüller, R. K.; Carpenter, A. E.; Wessling, M.; Post, G. F.; Uetz, M.; Reinders, M. J. T. An Algorithm-Based Topographical Biomaterials Library to Instruct Cell Fate. *Proc. Natl. Acad. Sci. U. S. A.* **2011**, *108* (40), 16565−16570.
(62) Carvalho, A.; Pelaez-Vargas, A.; Hansford, D. J.; Fernandes, M. H.; Monteiro, F. J. Effects of Line and Pillar Array Microengineered SiO2 Thin Films on the Osteogenic Differentiation of Human Bone Marrow-Derived Mesenchymal Stem Cells. *Langmuir* **2016**, *32* (4), 1091−1100.
(63) Geiger, B.; Spatz, J. P.; Bershadsky, A. D. Environmental Sensing through Focal Adhesions. *Nat. Rev. Mol. Cell Biol.* **2009**, *10* (1), 21−33.
(64) Maniotis, A. J.; Chen, C. S.; Ingber, D. E. Demonstration of Mechanical Connections between Integrins, Cytoskeletal Filaments, and Nucleoplasm That Stabilize Nuclear Structure. *Proc. Natl. Acad. Sci. U. S. A.* **1997**, *94* (3), 849−854.
(65) Dalby, M. J.; Riehle, M. O.; Yarwood, S. J.; Wilkinson, C. D. W.; Curtis, A. S. G. Nucleus Alignment and Cell Signaling in Fibroblasts: Response to a Micro-Grooved Topography. *Exp. Cell Res.* **2003**, *284* (2), 272−280.
(66) Abagnale, G.; Steger, M.; Nguyen, V. H.; Hersch, N.; Sechi, A.; Joussen, S.; Denecke, B.; Merkel, R.; Hoffmann, B.; Dreser, A. Surface Topography Enhances Differentiation of Mesenchymal Stem Cells towards Osteogenic and Adipogenic Lineages. *Biomaterials* **2015**, *61*, 316−326.
(67) Csaszar, E.; Kirouac, D. C.; Yu, M.; Wang, W.; Qiao, W.; Cooke, M. P.; Boitano, A. E.; Ito, C.; Zandstra, P. W. Rapid Expansion of Human Hematopoietic Stem Cells by Automated Control of Inhibitory Feedback Signaling. *Cell Stem Cell* **2012**, *10* (2), 218−229.
(68) Yim, E. K. F.; Pang, S. W.; Leong, K. W. Synthetic Nanostructures Inducing Differentiation of Human Mesenchymal Stem Cells into Neuronal Lineage. *Exp. Cell Res.* **2007**, *313* (9), 1820−1829.
(69) Tay, C. Y.; Yu, H.; Pal, M.; Leong, W. S.; Tan, N. S.; Ng, K. W.; Leong, D. T.; Tan, L. P. Micropatterned Matrix Directs Differentiation of Human Mesenchymal Stem Cells towards Myocardial Lineage. *Exp. Cell Res.* **2010**, *316* (7), 1159−1168.
(70) Mathieu, P. S.; Loboa, E. G. Cytoskeletal and Focal Adhesion Influences on Mesenchymal Stem Cell Shape, Mechanical Properties,

DOI: 10.1021/acsami.7b08237
ACS Appl. Mater. Interfaces 2017, 9, 31433−31445

and Differentiation down Osteogenic, Adipogenic, and Chondrogenic Pathways. *Tissue Eng., Part B* **2012**, *18* (6), 436−444.

DOI: 10.1021/acsami.7b08237
ACS Appl. Mater. Interfaces 2017, 9, 31433−31445